Noname manuscript No.
(will be inserted by the editor)

Future Regional Projections of Extreme Temperatures in Europe: A Nonstationary Seasonal Approach

M. D. Frías · R. Mínguez · J. M. Gutiérrez · F. J. Méndez

Received: date / Accepted: date

Abstract In recent years, there has been an increasing interest in studying the impacts of climate extremes in different sectors (agriculture, energy, insurance, etc.). In particular, extreme temperatures and heat waves have had a big impact in European socioeconomic activities during the last years (e.g. the 2003 heat wave in France). One of the reasons which makes the scientific community believe in climate change is that the prevalence and severity of extremes is changing, thus giving rise to more severe impacts with unpredictable consequences. For this reason, the development of methods and tools to analyze extremes in climate change context is of great interest. Regional climate models offer the opportunity to analyze and project in different future scenarios the variability of extremes at regional time scales. In the present work, we estimate changes of maximum temperatures in Europe using two state-of-the-art regional circulation models from the EU ENSEMBLES project. Regional climate models are used as dynamical downscaling tools to provide simulations on smaller scales than those represented for global climate models. Extremes are studied using a time-dependent generalized extreme value (GEV) model for monthly maxima, which allows analyzing different time-scale return periods (monthly, seasonal, annual, etc.). The study focuses on the end of the 20th century (1961-2000), used as a calibration/validation period, and analyzes the changes projected for the period 2061-2100 considering the A1B emission scenario. Finally, we analyze all over Europe the exceptionality of two well-known extraordinary events: i) the 2003 summer and ii) 2006 autumn.

M. D. Frías
Department of Applied Mathematics and Computer Science. Universidad de Cantabria. Avd. de los Castros s/n, Santander, 39005 Spain.
Tel.: +34 942203948
E-mail: friasmd@unican.es

R. Mínguez
Environmental Hydraulics Institute *IH Cantabria*, Universidad de Cantabria. Avd. de los Castros s/n, Santander, 39005 Spain.

J. M. Gutiérrez
Instituto de Física de Cantabria, CSIC-UC. Santander, 39005 Spain.

F. J. Méndez
Environmental Hydraulics Institute *IH Cantabria*, Universidad de Cantabria. Avd. de los Castros s/n, Santander, 39005 Spain.

Keywords extreme temperature · Europe · Regional Models · ENSEMBLES · non-stationary GEV · Return values

1 Introduction

The major floods and heat waves registered in several regions of the world over the last decade —e.g. the 2003 summer heat wave over Europe (Shär and Jendrithzky, 2004)— have shown the enormous consequences of these extreme events on society and ecosystems. Moreover, there is growing evidence that climate change has the potential to alter the frequency and intensity of extremes, thus driving more severe events with unpredictable consequences (Kharin and Zwiers, 2005; Tebaldi et al, 2006). Therefore, the projection of climate extremes under different future scenarios is a crucial information to assess the potential impacts of climate change on human and natural systems, which are more sensitive to changes in the extremes than in the mean climate (see, e.g. Kunkel et al, 1999).

Nowadays, the main tools available for this task are the ensembles of global (Meehl et al, 2007) and regional (Christensen et al, 2007) climate model simulations (referred to as GCMs and RCMs, respectively), produced by the international climate modeling community in the framework of different international projects. These models have a characteristic resolution of 250 and 25 km, respectively, and the resulting simulations project the climate according to different emission scenarios for the XXI century, providing also an estimation of the underlying uncertainty. In particular, the EU-funded project ENSEMBLES (van der Linden and Mitchell, 2009) is an example of a major international effort to provide, among other things, a coordinated multi-RCM ensemble of regional projections over Europe, considering both a ERA40-forced control period (1960-2000) and A1B scenarios (2001-2100) using forcings from different GCMs. The analysis of this dataset has focused mainly on the mean climate (see the special volume Kjellstrom and Giorgi, 2010) and on particular proxy indicators of extreme behavior (see, e.g. Fischer and Schar, 2010; Herrera et al, 2010, for an study over Europe and over the Iberian peninsula, respectively).

The statistical theory of extreme values (Coles, 2001) provides the mathematical framework for modeling the tail distribution of climate variables, i.e. the extreme values, allowing us to obtain useful information such as return values for certain return periods. For instance, the generalized extreme value (GEV) distribution has been used in different climate studies to model block extremes, typically annual maxima or minima, both in observed and simulated data (Kharin et al, 2005; Goubanova and Li, 2007; Kioutsioukis et al, 2010). In particular, the recent study by Nikulin et al (2011) applies the GEV distribution considering annual maxima to one of the ENSEMBLES models described above, forced by several GCMs in future climate conditions. As a result, for instance, they report annual 20-year return values for maximum temperatures for control and future scenarios.

Recent advances in extreme value theory allow introducing time-dependent variations in the GEV models considering different non-stationary mathematical frameworks where parameters are replaced by functions dependent of time of different forms (Coles, 2001). In a simple setting, the parameters can include a trend term varying linearly with time (Cooley, 2009) or a forcing term varying with some external climatic indices like the Southern Oscillation Index or the North Atlantic Oscillation (NAO). For instance Kharin and Zwiers (2005) applied a GEV distribution with parameters depending lin-

early on time to analyze global changes in temperature and precipitation from global climate change simulations. There are also studies combining both approaches (Méndez et al, 2007; Brown et al, 2008); for instance, Brown et al (2008) studied global changes in extreme daily temperature since 1950 considering the existence of trends and the influence of the NAO. More complex approaches consider harmonic functions reflecting the seasonality of the occurrence of maxima. For instance, Menéndez et al (2009); Izaguirre et al (2010) developed a time-dependent model based on the GEV distribution that accounts for the seasonality and interannual variability of extreme wave height. In this case, the non-stationary behavior is parameterized using functions of time (harmonic functions and covariates) for the parameters of the distribution. A similar approach has been considered by Rust et al (2009) to model extreme precipitation in the UK on a seasonal basis.

The purpose of the present study is twofold. First, we introduce a non-stationary seasonal GEV distribution with time-dependent harmonic location, scale and shape parameters fitted to data considering monthly extremes. As we show, this method is suitable to reflect the different impact of climate change in the extreme temperatures on the different seasons. Then, the resulting model is applied to estimate seasonal return values of maximum temperatures over Europe considering both the reanalysis-driven regional simulations (1961-2000) and future projections (2061-2100) driven by A1B scenario simulations. The former are used to validate the model and to estimate the biases corresponding to regional models and the later is used to infer the projected return values in a changing climate. Simulations from the RCMs are compared to the observed natural variability reflected by the E-OBS dataset which is the state-of-the-art publicly available high-resolution daily dataset for Europe (Haylock et al, 2008). This work is done using two regional models from the state-of-the-art ENSEMBLES dataset of regional climate simulations. The combination of these two purposes is addressed to increase the current knowledge of temperature extremes over Europe by means of the application of a non-stationary GEV model to high resolution simulations.

The outline of this paper is as follows. First we describe the different kind of maximum temperature data used in section 2. The non-stationary model is introduced in section 3 and is applied to observed extreme temperatures in section 4. The simulated warm temperature extremes for the end of the 20th century are validated against observations in section 5. Changes projected for the period 2061-2100 are also presented in that section. The main findings of the study are summarized in section 6.

2 Observed and model data

In this paper we analyze the control and transient simulation of two RCMs from the EU funded ENSEMBLES project (http://www.ensembles-eu.org), which aimed at the generation of climate change scenarios over Europe. ENSEMBLES studied regional climate change from different perspectives and includes a large variety of communities and state-of-the-art methodologies and techniques. In particular, dynamical downscaling of GCM simulations, both control and transient, was performed using nine different RCMs run by different institutions over a common area covering the entire continental European region and with a common resolution of 25 km; some of the models where also run at a 50km resolution in order to explore the added value of the resolution increase (as far as we know, no result on issue has been reported yet). More information on the experiments performed can be found in van der Linden and Mitchell (2009). In

particular, in this paper we consider the following experiments run in the framework of this project: (1) All RCMs were run driven by re-analysis data from the European Centre for Medium Range Weather Forecasts (ECMWF) as boundary conditions (see Uppala and others (2005) for more details about the ERA40 reanalysis); (2) the RCMs were driven by control climate scenario (20c3m) simulations from different GCMs, (3) the RCMs where also drive by future (A1B scenario) simulations from the same GCMs. The analysis of these experiments will allow us estimating different sources of errors and biases in the projections: data from (1) allows to estimate the RCM bias in perfect boundary conditions (optimal conditions). Comparing (2) and (1) we can estimate whether the bias pattern is robust in sub-optimal conditions (GCM simulations). If this is the case, then we can apply the standard "delta method" and compute the projected RCM anomaly as the difference of the future and control projections (this different would remove the RCM bias out of the regional change signal, extrapolating to changing conditions the robustness of the bias pattern obtained in suboptimal conditions).

In this paper, we consider monthly maximum temperature data from the Koninklijk Nederlands Meteorologisch Instituut (KNMI) and the Swedish Meteorological and Hydrological Institute (SMHI). The selection of these RCMs is based on two criteria. On one hand the period simulated for these models using the ERA40 reanalysis as boundary conditions is longer than for other RCMs. In ENSEMBLES all the RCMs were run over a common period (1961-1990), however some of them simulated longer periods. Simulations from KNMI and SMHI models cover a common period from 1961 to 2000. On the other hand, not all the GCMs considered in ENSEMBLES were nested into every RCM. The above two RCMs were forced with driving conditions from the same global model and, thus, conclusions should be attributed to the regional model behavior, not to differences with the GCM considered. The two regional models were run using the ECHAM5 GCM for a common period from 1961 to 2100. In this study, the period analyzed for the future projections extends from 2061 to 2100.

For the purposes of validation of the RCM simulations in present climate, monthly maximum temperature data from the E-OBS grid are considered from 1961 to 2000. The E-OBS dataset is a high-resolution gridded dataset developed in ENSEMBLES for maximum temperature, among other surface variables, and it is provided at both 50 and 25km original resolution. This dataset improves previous gridded data over Europe in the number of stations used, being the best publicly available gridded product for Europe to date. However, since station coverage is not homogeneous in space due to data availability/sharing limitations, some problems of lack of representativeness have been pointed out, particularly for extremes (see, e.g. Hofstra et al, 2010; Herrera et al, 2010). Therefore, in this work we consider the observation grid and RCM simulations with the lower 50km resolution. This choice is also convenient from a computational point of view, since the parameters of the seasonal GEV model should be optimized at a grid box level (note that the 50km grid contains a total of 6271 grid boxes over Europe). See Haylock et al (2008) for more details about the characteristics of E-OBS dataset and the methodology applied.

3 Nonstationary Seasonal GEV model

A GEV model with time-varying location (μ_t), scale (ψ_t), and shape (ξ_t) parameters is called a nonstationary GEV model (Coles, 2001) and is given by the following

cumulative distribution function (CDF):

$$G(x_t;\mu_t,\psi_t,\xi_t)=\begin{cases}\exp\left\{-\left[1+\xi_t\left(\dfrac{x_t-\mu_t}{\psi_t}\right)\right]_+^{-\dfrac{1}{\xi_t}}\right\};\xi_t\neq 0,\\ \exp\left\{-\exp\left[-\left(\dfrac{x_t-\mu_t}{\psi_t}\right)\right]\right\};\xi_t=0,\end{cases}\tag{1}$$

where $[a]_+=\max(0,a)$.

The GEV family includes three distributions corresponding to the different types of tail behavior: Gumbel ($\xi_t=0$) with a light tail decaying exponentially; Fréchet distribution ($\xi_t>0$) with a heavy tail decaying polinomially, and Weibull ($\xi_t<0$) with a bounded tail. The corresponding time dependent quantiles $x_{q,t}$ are:

$$x_{q,t}=\begin{cases}\mu_t-\frac{\psi_t}{\xi_t}\left[1-(-\log q)^{-\xi_t}\right], \text{ if } \xi_t\neq 0,\\ \mu_t-\psi_t\log(-\log q), \qquad \text{if } \xi_t=0,\end{cases}\tag{2}$$

where q is the corresponding probability.

In addition to "instantaneous" time dependent quantiles as given in (2), it is of great interest the calculation of "aggregated" time dependent quantiles, which would allow us the calculation of different annual return levels $\bar{x}_q$ associated with periods equal to or longer than one month using the same model. Thus, assuming a period given by the interval (t_a,t_b), the annual return levels $\bar{x}_q$ can be obtained solving the following implicit equation: [►OJO: El producto es sobre indices discretos y no queda claro que los tiempo se refieran a "meses" o "dias"]

$$q=\prod_{t=t_a}^{t_b}G(\bar{x}_q;\mu_t,\psi_t,\xi_t),\tag{3}$$

which can be approximated by:

$$q=\exp\left\{-k_m\int_{t_a}^{t_b}f(\bar{x}_q,t)dt\right\},\tag{4}$$

where $k_m=12$ and the function $f(\bar{x}_q,t)$ is equal to:

$$f(\bar{x}_q,t)=\begin{cases}\left[1+\xi_t\left(\frac{\bar{x}_q-\mu_t}{\psi_t}\right)\right]^{-1/\xi_t}; \text{ if } \xi_t\neq 0\\ \exp\left[-\left(\dfrac{\bar{x}_q-\mu_t}{\psi_t}\right)\right]; \qquad \text{if } \xi_t=0.\end{cases}$$

In this paper, expression (4) is used to calculate annual return levels related to: the whole year, spring, summer, autumn and winter, respectively. The advantage of the proposed formulation is that there is no need to treat data and fitting for each period separately, reducing the uncertainty in the estimation of seasonal and annual return values.

3.1 Model Formulation

Several nonstationary models have been recently introduced to deal with trends and interannual oscillations (see, for instance, Mínguez et al (2010b)). In this study, we consider a non-stationary model for seasonal variations introduced in Menéndez et al (2009), hence dealing with the intra-annual (seasonal) variations of temperature maxima. Within this approach, monthly maximum temperatures x_t of successive months are assumed to be independent random variables following a GEV distribution with time-dependent parameters as in (1). To introduce seasonality, the model proposed in Menéndez et al (2009) is stated as follows:

$$\mu_t = \beta_0 + \sum_{i=1}^{P_\mu} \left[\beta_{2i-1}\cos(iwt) + \beta_{2i}\sin(iwt)\right] \tag{5}$$

$$\log(\psi_t) = \alpha_0 + \sum_{i=1}^{P_\psi} \left[\alpha_{2i-1}\cos(iwt) + \alpha_{2i}\sin(iwt)\right] \tag{6}$$

$$\xi_t = \gamma_0 + \sum_{i=1}^{P_\xi} \left[\gamma_{2i-1}\cos(iwt) + \gamma_{2i}\sin(iwt)\right], \tag{7}$$

where t is given in years, $\log(\psi_t)$ ensures positiveness of the scale parameter ($\psi_t > 0$), β_0, α_0, and γ_0 are mean values, β_i, α_i, and γ_i are the amplitudes of harmonics considered in the model, $w = 2\pi/T$ is the angular frequency, T is one year, and P_μ, P_ψ and P_ξ are the number of sinusoidal harmonics to be considered within the year, associated with the location, scale and shape parameters, respectively. The resulting parameters are estimated using the method of maximum likelihood, where the log-likelihood function is defined as follows:

$$\begin{aligned}\ell(\boldsymbol{\theta};\boldsymbol{x},\boldsymbol{t},\boldsymbol{c}) &= \sum_{t=1}^{n_d}\log(g(x_t;\mu_t,\psi_t,\xi_t)) \\ &= -\sum_{t=1}^{n_d}\begin{cases}\log\psi_t + \left(1+\dfrac{1}{\xi_t}\right)\log z_t + z_t^n, & \text{if } \xi_t \neq 0, \\ \log\psi_t + \dfrac{x_t-\mu_t}{\psi_t} + \exp\left(-\dfrac{x_t-\mu_t}{\psi_t}\right), & \text{if } \xi_t = 0,\end{cases}\end{aligned} \tag{8}$$

where $\boldsymbol{x} = (x_1, x_2, \ldots, x_{n_d})^T$ is the sample vector, n_d is the number of monthly maxima observations, $z_t = 1+\xi_t\left(\dfrac{x_t-\mu_t}{\psi_t}\right)$ and $z_t^n = z_t^{-1/\xi_t}$ are auxiliary variables to simplify the computational implementation, and $g(x_t;\mu_t,\psi_t,\xi_t) = \frac{dG(x;\mu_t,\psi_t,\xi_t)}{dx}$ is the GEV probability density function (PDF).

Although sophisticated methods have been proposed for the automatic selection of harmonics (e.g. Mínguez et al, 2010a, present a method based on Akaike information criterion), they would require a prohibitive computational time to be applied to the whole European domain considered in this paper, with 6271 grid points. For this reason we selected the following fixed parameterization for all cases (grid points) by comparing the results of different models for a reduced number of locations or cities (Athens, Brussels, Copenhagen, Lisbon, London, Madrid, Oslo, Paris, Rome, Stockholm) using the E-OBS dataset (1961-2000):

$$P_\mu = 3,\ P_\psi = 3,\ \text{and } P_\xi = 1. \tag{9}$$

The reason to take this parameterization is threefold: i) it is the most complex model with all the parameters being statistically significant on a 5% level for the test cases performed, ii) we get very good diagnostics for all cases, and iii) it is flexible enough to capture the possible spatial variations over the grid.

The harmonic in the shape parameter ξ was introduced to check whether the tail behavior changes with season. Results are given in Figure 1, where the intra-annual evolution of the shape parameter is shown for each city. Note that the parameters allow the model to fit the particular tail behavior for each location. This figure shows that the tail behavior is Weibull ($\xi < 0$) for all cities (bounded tail behavior). Note that the shape parameter is statistically significant (90% confidence intervals does not contain the zero), with a clear seasonality effect, excluding in Paris where a constant shape parameter could be used instead. Since we aim at a common model for all grid points we decided to use the model with an harmonic in the shape parameter, although we are aware that shape parameter may be difficult to estimate due to lack of information in the tails.

Figure 2 shows the seasonal evolution of the location parameter (solid lines) and 95% "instantaneous" time dependent percentile $x_{0.95,t}$ (dashed line) [►OJO: no se distingue la linea discontinua] in the resulting model for all cities, capturing the seasonal variations. Note that both location and 95% percentile are conditional on the time of occurrence within the year.

An important issue about the selected model is the decision about not to include parameters accounting for possible trends. One of the aims of the paper is to make a comparison between the fitting using two different periods (1961-2000 and 2061-2100), in order to check i) how the regional climate models perform with respect to maxima observations, and ii) their suitability to be used for the estimation of return levels in the future. For this reason, we decided to fit results from models for those periods independently and without including trends, this strategy allow us to get unique return level values for each period to make a fair comparison. Nevertheless, we are aware of the possibility of including trends in the model, which is a subject for further research.

3.2 Diagnostics

A number of diagnostic statistics and plots were computed to assess the goodness of fit of the resulting models in the selected cities. In particular we computed quantile-quantile (Q-Q, see Figure 3)) and probability-probability (P-P, not shown due to space limitations) plots, obtaining very good diagnostics, with points close to the diagonal. Note that P-P and Q-Q plots for the sample of computed values $\bar{z}_t$ can be obtained as $\bar{z}_t = \frac{1}{\xi_t} \log\left[1 + \xi_t \left(\frac{x_t - \mu_t}{\psi_t}\right)\right]$, so that if $\bar{z}_{(1)}, \bar{z}_{(2)}, \ldots, \bar{z}_{(n_d)}$ are the corresponding sample order statistics, the plotting points for the probability plot are $\{i/(n_d+1),\ \exp(-\exp(-\bar{z}_{(i)}))\}$ whilst the plotting points for the quantile plot are $\{-\log(-\log(i/(n_d+1))),\ \bar{z}_{(i)}\}$. Dashed lines in Figure 3 [►OJO: es dashed? no se distingue] indicate 90% confidence intervals.

Using the resulting models, we have also calculated annual and seasonal aggregated return levels (4) for the test cities, which provide the knowledge about the mean number of years, springs, summers, autumns and winters, respectively, in which a given threshold is exceeded. Note that this information is obtained using only one fitted model for each location. In addition, and in order to compare the robustness of the

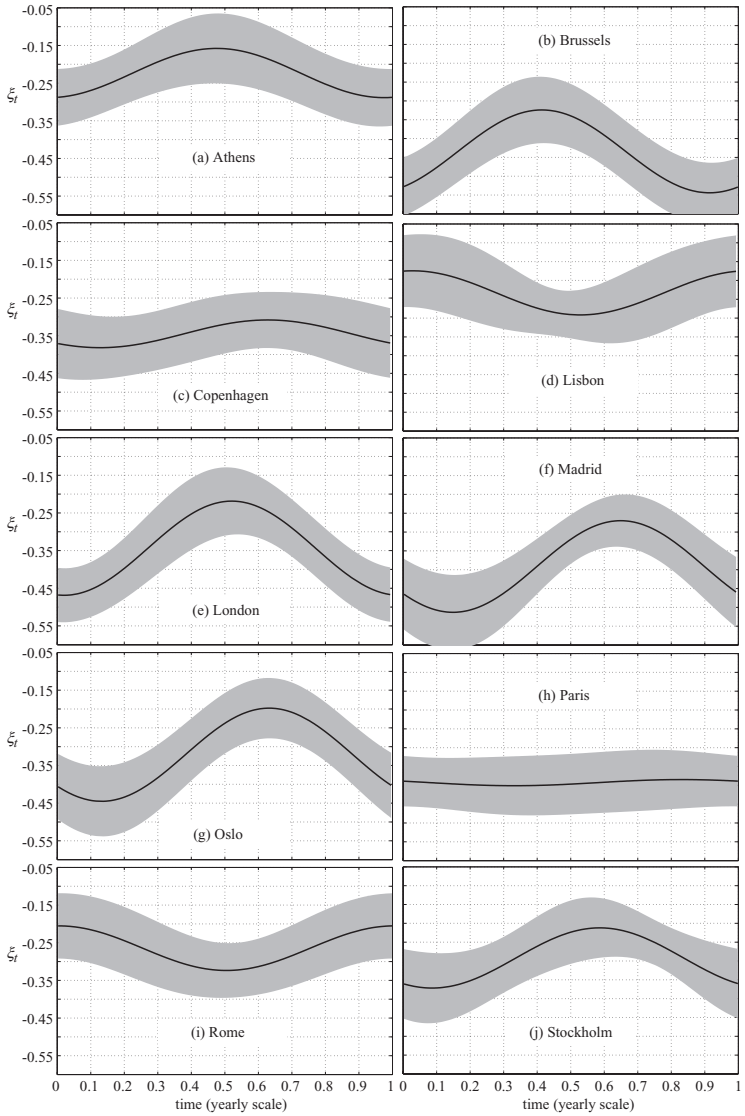

Fig. 1 Goodness of fit plots for the maximum monthly temperature shape parameter, related to the EOBS database, at the selected locations. Shading indicates 90% confidence intervals.

results, we also computed the annual return level plots using the traditional stationary approach where only yearly maximum data values are considered. The following information is shown in Figure 4:

– Fitted annual return levels (red line) obtained using the non-stationary model, and 90% confidence bands (red dashed lines [►OJO: apenas se aprecia este intervalo de confianza? o es que se solapa con el estacionario?]). Empirical annual return period quantiles (red dots) are also shown, where only the maximum value for each year is used.

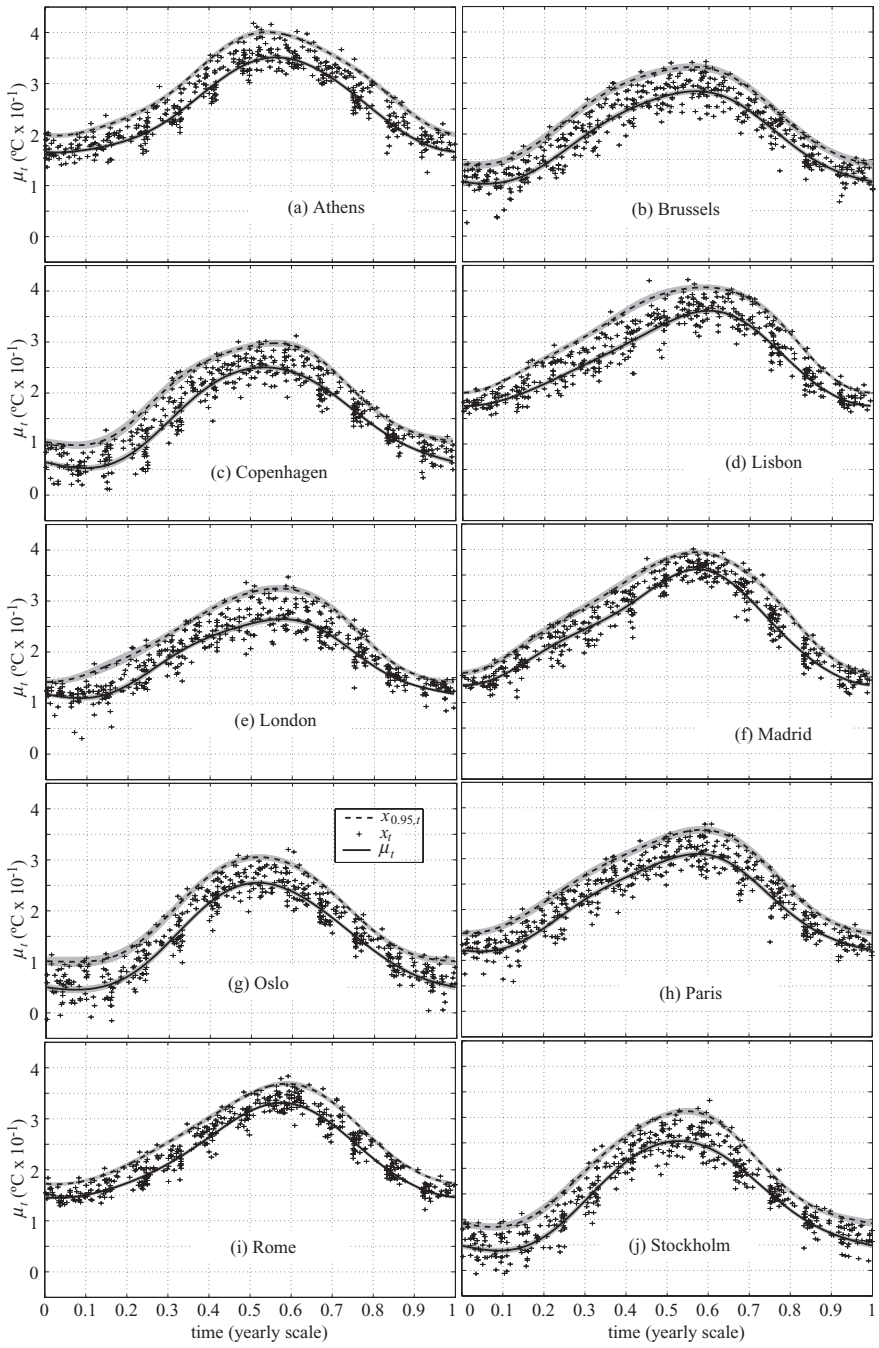

Fig. 2 Goodness of fit plots for the maximum monthly temperature location parameter (continuous line) and 0.95 time dependent quantile ($x_{0.95,t}$, dashed line) for the selected locations (in different panels). Shading indicates 90% confidence intervals.

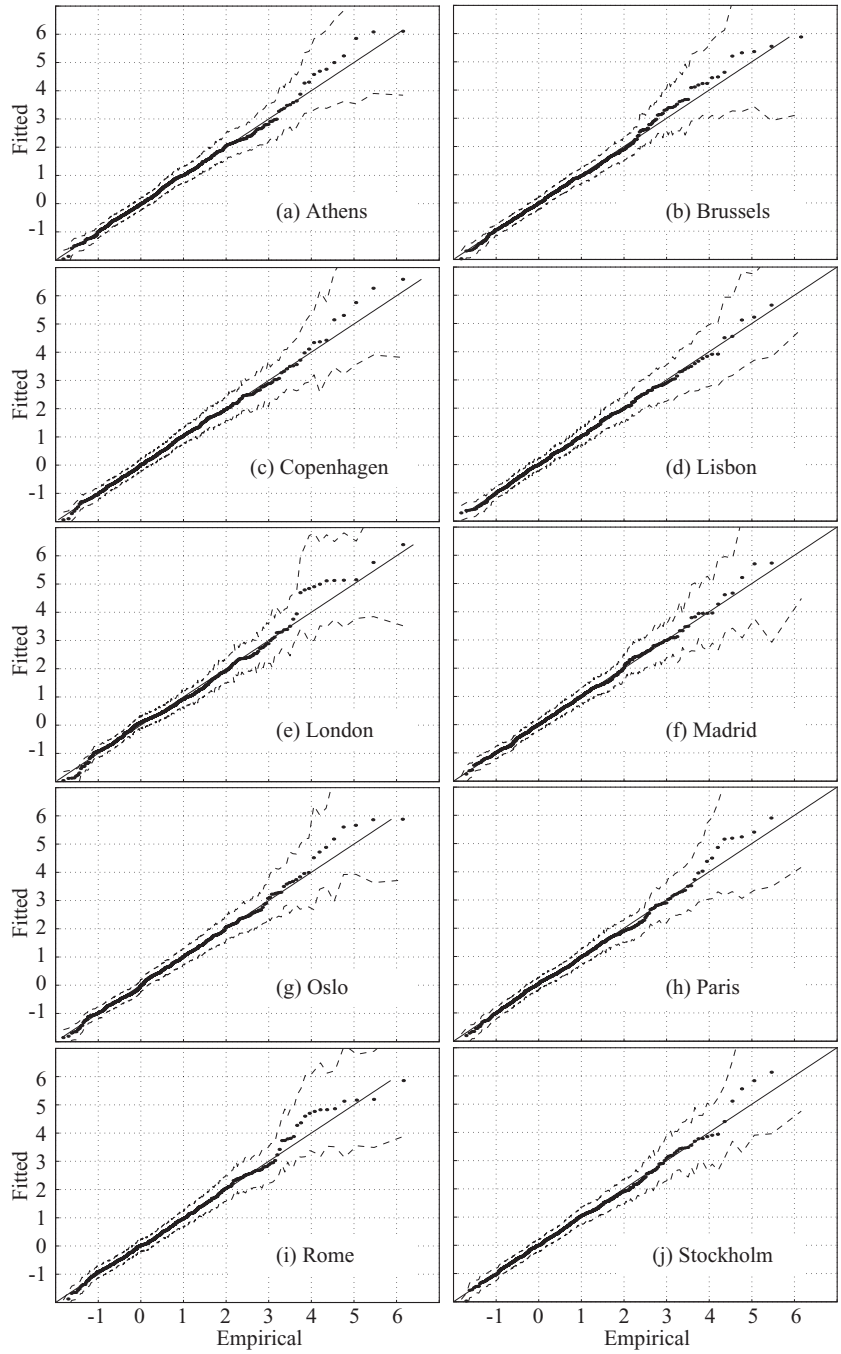

Fig. 3 Goodness of fit Q-Q plots for the selected cities. Dashed lines indicate 90% confidence intervals.

– Fitted and empirical return levels for: i) spring (green line and dots, respectively), ii) summer (blue line and dots, respectively), iii) autumn (black line and dots, respectively), and iv) winter (gray line and dots, respectively). All of them obtained using the non-stationary model. Note that empirical points have been calculated considering maximum values for each spring, summer, autumn and winter, respectively.
– To check model performance, we have also plotted return levels from the traditional stationary GEV based on annual block maxima (black dot-dashed line [►OJO: black or grey??]).

The above figures provide some interesting information. Since the annual maxima occurs during the summer, annual aggregated quantiles coincide with summer aggregated quantiles for all cities. This result shows the consistency and coherency of the proposed model. Note that blue lines associated with summer are hidden behind annual red lines. The goodness of fit of the selected model is also justified through the comparison with the results using the stationary approach based on annual maxima. Results from this model are plotted using black dashed lines. Note that in all cases, this line is almost undistinguishable with respect to results from the non-stationary approach. This confirms the validity, consistency and coherency of the proposed model.

Over Europe, the minimum maximum temperatures are always obtained during winter. Note that gray lines related to winter are below the rest of the seasonal quantiles. Autumn presents different maximum temperatures with respect to spring. Higher for Athens, Lisbon, London, Madrid, Paris and Rome, and lower for Copenhagen, Oslo and Stockholm. This clearly indicates that springs present higher maximum temperatures than autumns in the South-East part of Europe and United Kingdom, whereas in the North-West part autumns present higher maximum temperatures than springs. For this particular case, Brussels is in the frontier where autumns and springs have similar maximum temperature behavior.

4 Results for Observed Extreme Temperatures

In this section we apply the seasonal GEV model introduced Sec. 3.1 (calibrated and diagnosed considering ten illustrative locations) to obtain maps of return values for the whole European domain. To this aim we consider the E-OBS maximum temperature daily data series in each of the 6271 resulting grid points for the 40-year period 1961-2000, and focus on return periods for 40 and 100 years; note that $T = 40$ mark the limit of the empirical available data, whereas $T = 100$ is far beyond the available data and fully relies in the extrapolation of the tail estimation. Note also that, in this study, the return value for a return period T on a particular "season" —defined arbitrarily as in (3)— is the extreme temperature value that is expected to be exceeded on average once every T years in that particular "season". Figure 5 presents a map of 40-year return levels for Spring to Winter over Europe. This figure shows a South-North gradient, especially in Autumn and Winter, with larger return levels in the South, especially over the Mediterranean, and lower values in the North-Western. In summer there are less differences between North and South and almost the whole continent shows 40-year return values in the range from 30 to $40^{\circ}C$. The same dominant pattern was obtained for return values associated with other return periods analyzed (20 and 100 years, not shown).

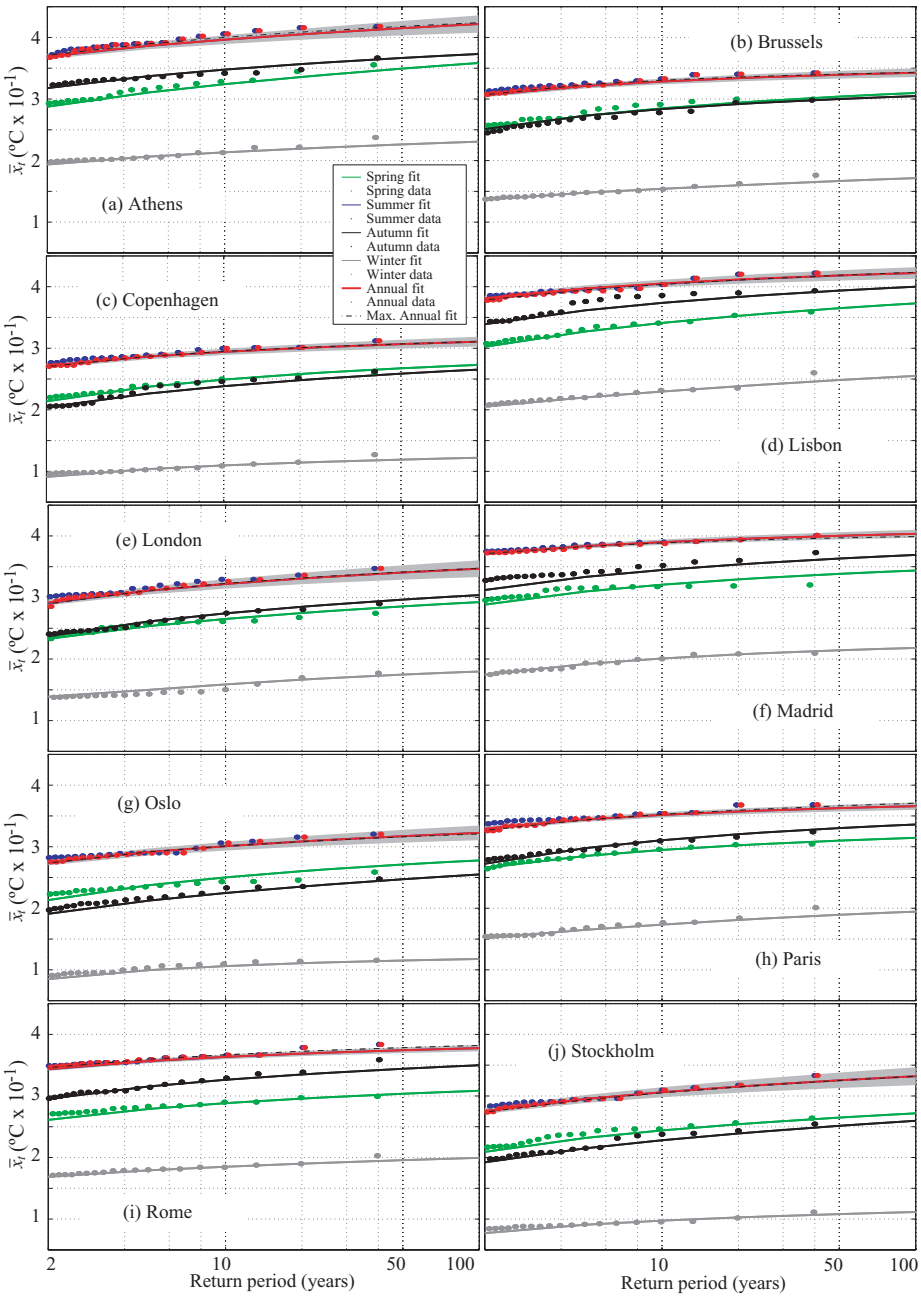

Fig. 4 Return level plots for the selected locations: summer, autumn, winter, spring, and annual using the non-stationary approach, and annual using annual maxima data. Red dashed lines indicate 90% confidence intervals for the annual quantile.

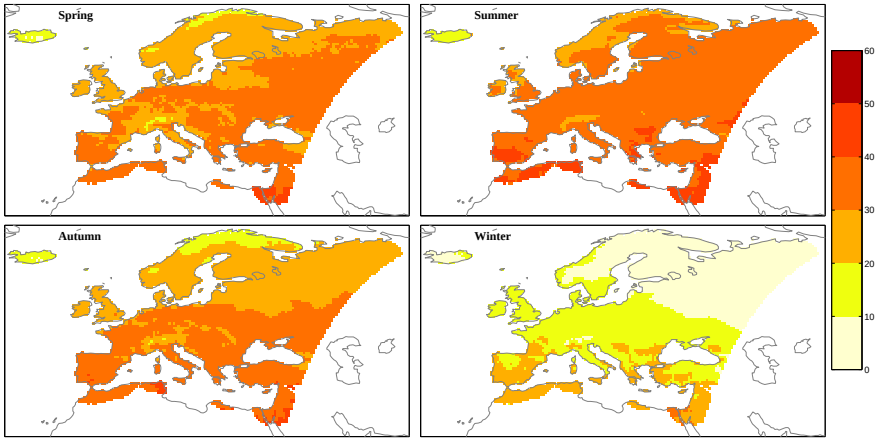

Fig. 5 40-year return values of extreme maximum temperature from the E-OBS dataset. The panels show the four seasons.

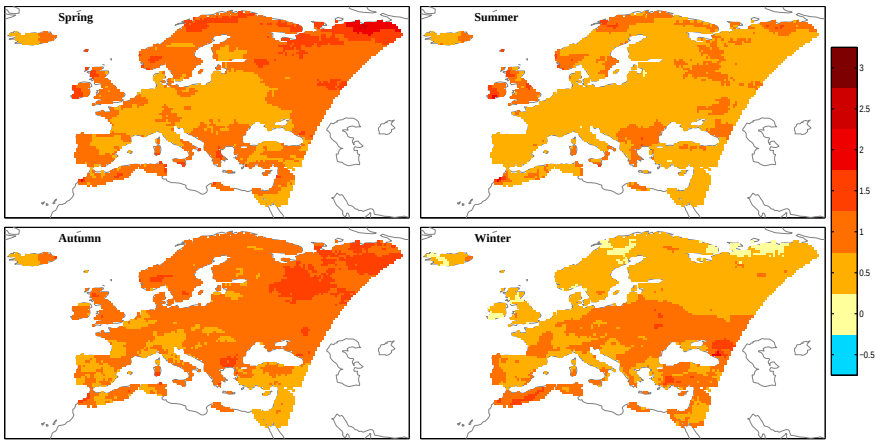

Fig. 6 Changes of 100-year return levels relative to 40-year return levels. Values calculated for extreme maximum temperature from the E-OBS dataset.

Figure 6 shows the differences of the 100-year return values relative to those obtained for a 40-year period. Higher values are found for the 100-year return levels for all seasons, although the increments are not high (the maximum increments achieved are $3°C$). In Spring and Autumn the differences are larger in the North-East whereas in Winter the maximum is mostly reached in regions over Central Europe. Differences are more homogeneous over the whole Europe in Summer due to the less strong meridional gradient of the return values found in this season for the different periods.

5 Results for RCM Simulated Extreme Temperatures

Once extremes from the E-OBS pseudo-observations have been analyzed, we focus on the results for the two RCMs considered in this work: KNMI and SMHI.

5.1 Extremes in a control period

Firstly, we analyze the simulations done in the control period 1961-2000, driven by both ERA40 (optimum conditions) and ECHAM5 20c3m scenario (sub-optimal conditions). The comparison of these results with those obtained for the observations in the previous section will provide a validation of the RCMs allowing identifying and removing systematic biases. The main goal is determining whether each RCM has a characteristic regional bias pattern which can be identified out of the global bias of the driving global model (ERA40 or ECHAM5) used as boundary conditions.

Maps for the 40-year return levels obtained for the KNMI and SMHI RCMs (both with ERA40 and ECHAM5 forcings) show a spatiotemporal pattern of return values similar as that obtained for the observed E-OBS dataset (not shown). A gradient of higher values in the South and lower values in the North is also found for the RCM simulations, attaining higher values also in Summer and lower in Winter. In order to quantify the degree of spatial agreement for the different return value patterns, we computed the Spearman's rank correlation between E-OBS and each RCM-GCM couple (e.g. KNMI forced by ERA40); the resulting values are shown in the diagram in Fig. 7 next to the arrows linking E-OBS with each of the RCMs. Note that in all the cases the correlations are over 0.80 indicating a good spatial agreement on the return values. In order to further explore the differences between the RCMs and the observations, Figure 8 shows the maps of biases between the RCM and the E-OBS values for each season (by rows) and RCM-GCM couple (by columns). Both KNMI and SMHI present a similar North-South gradient in the bias pattern, with return values overestimated over Southern Europe and underestimated in the North in Spring, Summer and Autumn. In Winter both models show a more uniform pattern with smaller bias, especially for the KNMI model. These changes are more pronounced for the SMHI model which registers lower values over a larger region with stronger negative differences in the North (around -5°C). A similar North-South gradient has been found by Nikulin et al (2011) for 20-yr return values of annual maximum temperature (summer in our study) applying a stationary GEV model to EOBS data and regional simulations from the RCA model forced by 6 GCMs. They also found a higher underestimation over Scandinavia which shown related to the fact that the stations considered in EOBS only represent the open-land temperature ignoring the forest influence in the maximum daytime temperature in a region with a large forest fraction.

An important result is that KNMI and SMHI models exhibit the same characteristic regional bias pattern (with small differences) for the two different global forcing conditions (reanalysis from ERA40 or control simulations from ECHAM5), so the inter-RCM variability of the bias pattern is much higher than the inter-GCM variability in the resulting patterns. In order to quantify the degree of spatial agreement for the different patterns, we computed the Spearman's rank correlation for the bias patterns (w.r.t. E-OBS) for each RCM-GCM couple; the resulting values are shown within the dashed box in the diagram in Fig. 7. For instance, in Spring (labelled as "P" in the diagram), the intra-RCM (for ERA40 and ECHAM5 forcings) correlations are 0.82 and 0.85 for the KNMI and SMHI models, respectively, whereas the inter-RCM (intra-GCM) correlations are 0.61 and 0.78, respectively. Note that the correlations between the global (ERA40 and ECHAM5) and regional (KNMI and SMHI) biases are much lower (0.37, 0.18, 0.45 and 0.44, for the respective combinations, also shown in the diagram in Fig. 7), thus indicating a robust regional pattern in the bias of the RCMs, when compared with the observations.

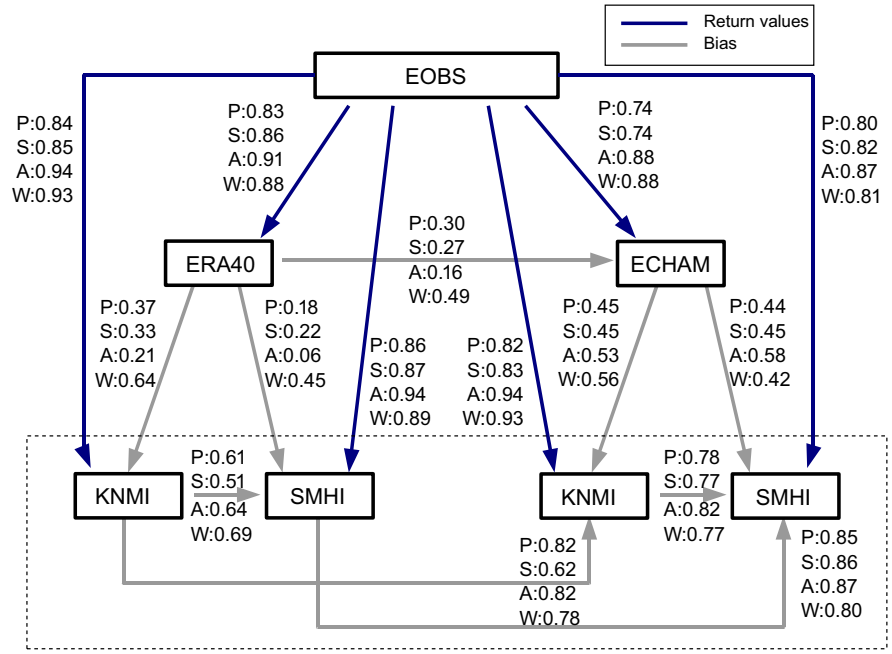

Fig. 7 Spearman's rank correlation among the maps of return values for the observations (EOBS), the driving global models (ERA40 and ECHAM5) and regional models (KNMI and SMHI). Black lines show correlations between the return values, whereas gray lines indicate correlations between the anomalies (biases) w.r.t. observations E-OBS. In each case, correlations are computed for each particular season: Spring (P), Summer (S), Autumn (A) and Winter (W).

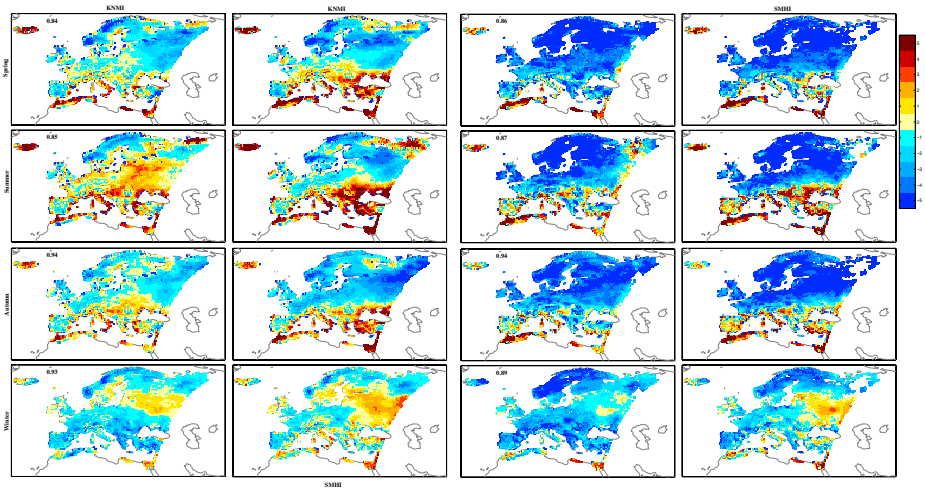

Fig. 8 Anomalies for the 40-year return values from the KNMI/SMHI models with respect to the E-OBS dataset. The first two columns correspond to the KNMI model (ERA40 and ECHAM5-20c3m forcings, respectively) whereas the last two columns show the corresponding plots for SMHI. Numbers on the panels show the spatial correlation of the RCMs and E-OBS return values.

5.2 Future changes in temperature extremes

We analyze the future changes in temperature extremes considering the RCMs driven by the ECHAM5 A1B emission scenario for the period 2061-2100. Since robust bias patterns have been identified for the RCMs in present climate conditions, we shall apply the "delta method" to obtain the estimated return values for future scenarios (see, e.g. Zahn and von Storch, 2010, and http://www.ipcc-data.org/ddc_change_field.html). This method consists on the comparison of simulated time slices of future scenarios relative to a simulated control scenario in the 20^{th} century (e.g. 20c3m scenario) of the same model. In the previous section we analyzed the return values obtained from the RCMs coupled to a control 20c3m scenario from ECHAM5 model. In this section we consider the RCM simulations driven by the future 2061-2100 time-slice output from ECHAM5 model for A1B scenario. Return levels corresponding to three return periods (20, 40 and 100 years) have been estimated using the methodology described in Sec. 3. Figure 9 presents the differences of the 40-year return values for the future A1B (2061-2100) relative to 20c3m present climate (1961-2000) simulations for the KNMI and SMHI models. It is found that changes in extreme temperature simulated by the two RCMs have very similar patterns revealing increase almost everywhere with the greatest magnitudes of the warming over Southern Europe. Other studies have also found this region more sensitive to climate change. For instance, the study by Nikulin et al (2011), presents an increase of temperature extremes in summer by the end of the century over all Europe with higher values in the South. Lower changes are registered in Winter in figure 9 which shows the larger differences in the North-West of Europe. The pattern of differences is almost the same for the other two return periods considered (not shown) being remarkable that the magnitude of the changes increases for longer return periods. Note also that model projections for the 21st century shows greater temperature extremes than the increase of temperature found in Figure 6 for the E-OBS data due to an increase of the return period.

Moreover, Fig. 10 shows the relative increment of the extreme values (40-year return values) with respect to the mean values (for daily maximum temperature), obtained as the ratio of the increments shown in Fig. 9 and the increments of the seasonal mean daily maximum temperatures computed in the same way. This figure shows that the increment for extremes is expected to be higher than for the mean seasonal temperatures, double in most of the European territory, particularly in Spring and Summer.

6 Conclusions

Two state-of-the-art regional circulation models from the EU ENSEMBLES project are considered to estimate changes of maximum temperatures in Europe. Extremes are studied in terms of return values using a time-dependent generalized extreme value model for monthly maxima. Seasonality is here introduced considering harmonic functions associated to the location, scale and shape parameters. The study focuses on the end of the 20th century (1961-2000), used as a calibration/validation period, and analyzes the changes projected for the period 2061-2100 considering the A1B emission scenario.

The robustness of the nonstationary model is compared to the traditional stationary approach revealing the consistency and coherency of the proposed model. This

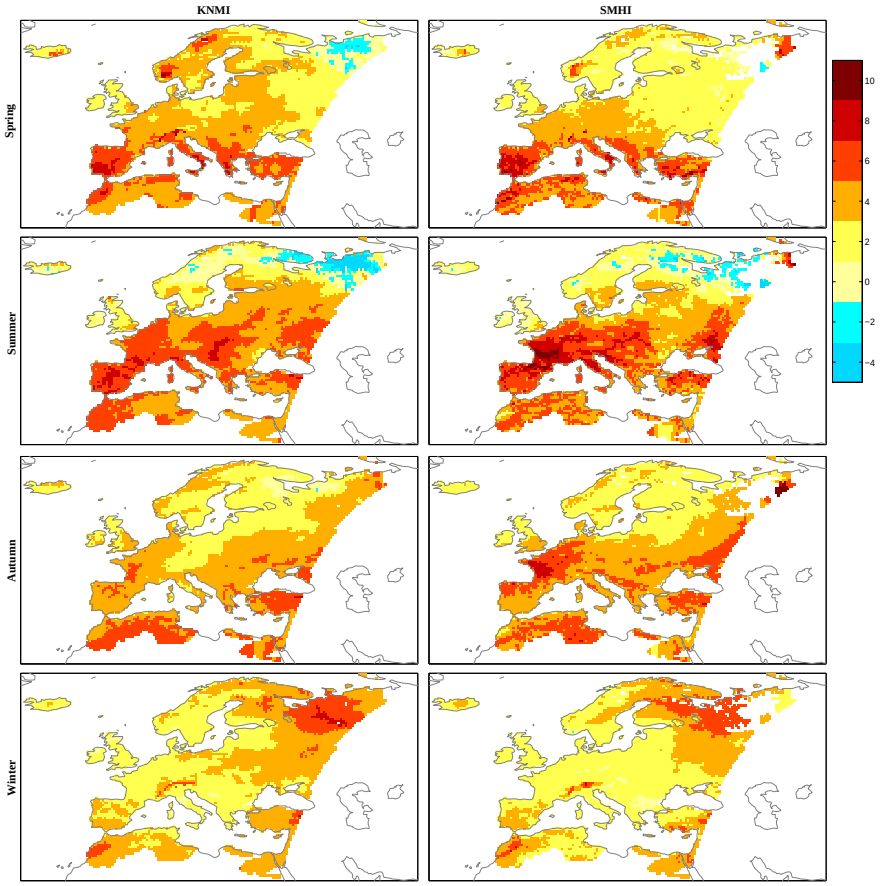

Fig. 9 Climate change responses for 40-year return levels in 2061-2100 relative to 1961-2000 simulated by the KNMI (left) and SMHI (right) RCMs, both driven by the ECMAH5 global model.

comparison also remarks the main advantage this approach versus the stationary GEV due to the no need to treat data and fitting for each period separately, reducing the uncertainty in the estimation of seasonal and annual return values.

Results for observed extreme temperatures from the E-OBS dataset (1961-2000) reveal a South-North gradient for the 40-year return value with larger values over the Mediterranean. Same pattern is found for the KNMI and SMHI simulations done in the control period driven by both ERA-40 and ECHAM5 20c3m scenario. It is also shown that KNMI and SMHI models exhibit the same characteristic regional bias pattern with respect to the E-OBS dataset (with small differences) for the two different global forcing conditions, so the inter-RCM variability of the bias pattern is much higher than the inter-GCM variability in the resulting patterns.

The projected future changes in temperature extremes in 2061-2100 relative to the control period reveals increase almost everywhere for both RCMs showing the greatest magnitudes of warming over Southern Europe. The magnitud of the changes increases for longer return periods. It is remarkable that model projections for the 21st century

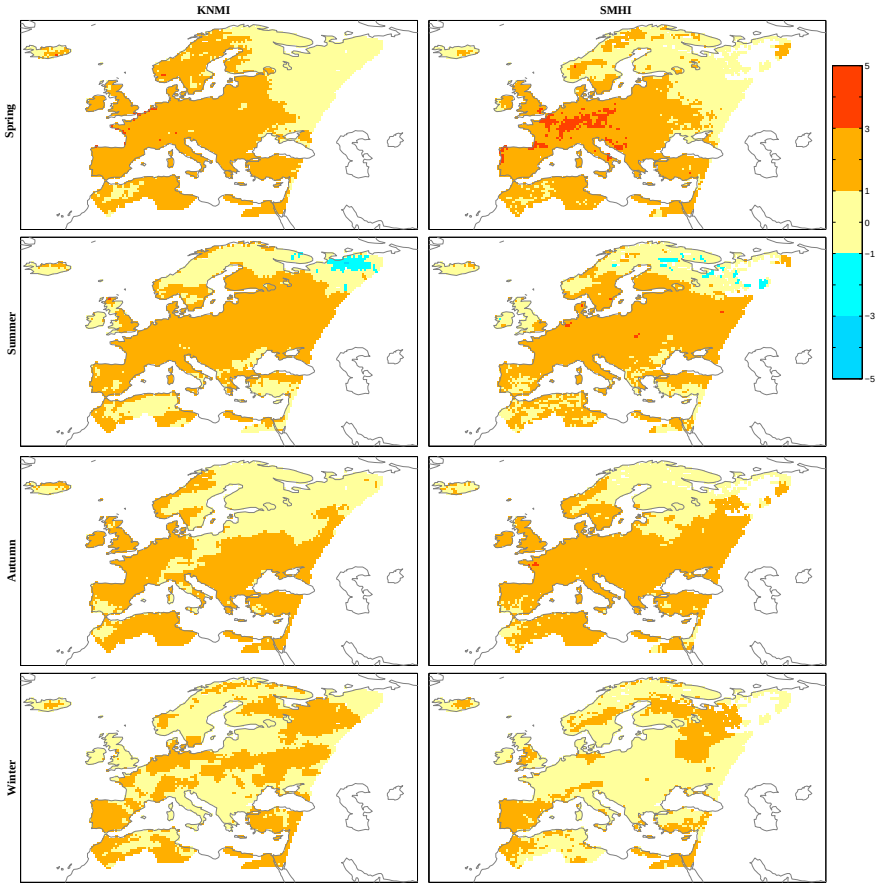

Fig. 10 As Figure 9, but relative to the increment of Tmax.

shows greater temperature extremes than the increase of temperature found for the E-OBS data due to an increase of the return period.

Acknowledgements The ENSEMBLES data used in this work was funded by the EU FP6 Integrated Project ENSEMBLES (Contract number 505539) whose support is gratefully acknowledged. We acknowledge the E-OBS data set and the data providers in the ECA&D project (http://eca.knmi.nl). R. Mínguez is indebted to the Spanish Ministry MICINN for the funding provided within the "Ramon y Cajal" program. This work was partly funded by projects "GRACCIE" (CSD2007-00067, Programa Consolider-Ingenio 2010), "AMVAR" (CTM2010-15009) and EXTREMBLES (CGL2010-21869) from Spanish Ministry MICINN, by project C3E (200800050084091) and ESCENA from the Spanish Ministry MARM, and by project MARUCA (E17/08) from the Spanish Ministry MF.

References

Brown SJ, Caesar J, Ferro CA (2008) Global changes in extreme daily temperature since 1950. J Geophys Res 113:D05,115

Christensen J, Hewitson B, Busuioc A, A Chen XG, Held I, Jones R, Kolli R, Kwon WT, Laprise R, Rueda VM, Mearns L, Menndez C, Risnen J, Rinke A, Sarr A, Whetton P (2007) Regional climate projections. In: Solomon S, Qin D, Manning M, Chen Z, Marquis M, Averyt K, Tignor M, Miller H (eds) Climate Change 2007: The Physical Science Basis. Contribution of Working Group I to the Fourth Assessment Report of the Intergovernmental Panel on Climate Change, Cambridge University Press, Cambridge

Coles S (2001) An Introduction to statistical modeling of extremes values. Springer, London

Cooley D (2009) Extreme value analysis and the study of climate change. a conebtart ib Wigley 1988. 97:77–83

Fischer E, Schar C (2010) Consistent geographical patterns of changes in high-impact european heatwaves. Nature Geoscience 3:398–403

Goubanova K, Li L (2007) Extremes in temperature and precipitation around the Mediterranean basin in an ensemble of future climate simulations. Global Planet Change 57:27–42

Haylock M, Hofstra N, Klein-Tank A, Klok EJ, Jones P, New M (2008) A European daily high-resolution gridded data set of surface temperature and precipitation for 1950–2006. J Geophys Res 113:D20,119

Herrera S, Fita L, Fernández J, Gutiérrez JM (2010) Evaluation of the mean and extreme precipitation regimes from the ensembles regional climate multimodel simulations over spain. J Geophys Res 115:D21,117, DOI 10.1029/2010JD013936

Hofstra N, New M, McSweeney C (2010) The influence of interpolation and station network density on the distribution and extreme trends of climate variables in gridded data. Climate Dyn 35:841–858

Izaguirre C, Méndez FJ, Menéndez M, Luceño A, , Losada IJ (2010) Extreme wave climate variability in southern europe using satellite data. Journal of Geophysical Research 115(–):–, DOI doi:10.1029/2009JC005802, to appear

Kharin VV, Zwiers FW (2005) Estimating extremes in transient climate change simulations. J Climate 18:1156–1173

Kharin VV, Zwiers FW, Zhang XB (2005) Intercomparison of near-surface temperature and precipitation extremes in AMIP-2 simulations, reanalyses and observations. J Climate 18:5201–5223

Kioutsioukis I, Melas D, Zerefos C (2010) Statistical assessment of changes in climate extremes over Greece (1955-2002). Int J Climatol 30:1723–1737

Kjellstrom E, Giorgi F (2010) Introduction. Climate Research 44:117–119

Kunkel KE, Andsager K, Easterling DR (1999) Long-term trends in extreme precipitation events over the conterminous United States and Canada. J Climate 12:2515–2527

van der Linden P, Mitchell J (eds) (2009) ENSEMBLES: Climate Change and its Impacts: Summary of research and results from the ENSEMBLES project. Met Office Hadley Centre, FitzRoy Road, Exeter EX1 3PB, UK

Meehl GA, Covey C, Delworth T, Latif M, McAvaney B, Mitchell JFB, Stouffer RJ, Taylor KE (2007) The WCRP CMIP3 multi-model dataset: A new era in climate change research. Bull Amer Meteor Soc 88:1383–1394

Méndez FJ, Menéndez M, Luceño A, Losada IJ (2007) Analyzing monthly extreme sea levels with a time-dependent GEV model. J Atmos Ocean Technol 24:894–911

Menéndez M, Méndez FJ, Izaguirre C, no AL, Losada I (2009) The influence of seasonality on estimating return values of signifcant wave height. Coastal Engineering 56:211–219

Mínguez R, Méndez FJ, Izaguirre C, Menéndez M, Losada IJ (2010a) Pseudo-optimal parameter selection of non-stationary generalized extreme value models for environmental variables. Environmental Modelling & Software 25:1592–1607, DOI DOI: 10.1016/j.envsoft.2010.05.008

Mínguez R, Menéndez M, Méndez FJ, Losada IJ (2010b) Sensitivity analysis of time-dependent generalized extreme value models for ocean climate variables. Advances in Water Resources 33:833–845, 10.1016/j.advwatres.2010.05.003

Nikulin G, Kjellstrom E, Hansson U, Strandberg G, Ullerstig A (2011) Evaluation and future projections of temperature, precipitation and wind extremes over Europe in an ensemble of regional climate simulations. Tellus 63(1):1–55, DOI 10.1111/j.1600-0870.2010.00466.x

Rust H, Maraun D, Osborn T (2009) Modelling seasonality in extreme precipitation. a UK case study. Eur Phys J 174:99–111

Shär C, Jendrithzky G (2004) The European heat wave of 2003: Was it merely a rare meteorological event or a first glimpse of climate change to come? probably both, is the answer, and the anthropogenic contribution can be quantified. Nature 432:559–560

Tebaldi C, Hayhoe K, Arblaster JM, Meehl GA (2006) Going to the extremes: an intercomparison of model simulated historical and future changes in extreme events. Climate Change 3-4:185–211

Uppala SM, et al (2005) The ERA-40 re-analysis. Quart J Roy Meteor Soc 131:2961–3012

Zahn M, von Storch H (2010) Decreased frequency of North Atlantic polar lows associated with future climate warming. Nature 467:309–312